Military Technical College
Kobry El-Kobbah,
Cairo, Egypt

6th International Conference
on
Chemical & Environmental
Engineering
29 -31 May, 2012.

## CPTA-1

# ELECTRODEPOSITION OF HIGH-MN ZINC-MANGANESE ALLOYS FROM CHLORIDE EECTROLYTE

M.Bučko[a], J.B.Bajat[b], B. Jokić[b]

## Abstract

Zinc-manganese alloys containing up to 40 at. % Mn were successfuly electrodeposited from a solution made of Zn and Mn chlorides, and boric acid. Cyclic voltammetry and chronoamperometry were used to clarify the influence of Mn salt concentration in the solution and deposition current density, on the kinetics of Zn-Mn electroreduction. Energy dispersive X-ray spectrometry was used to investigate a chemical composition of Zn-Mn deposits, and scanning electron microscopy was used for surface morphology analysis. It has been shown that the coatings possessing the highest Mn content, are with the surface morphology of high quality, and may be an adequate improvement of pure Zn coatings as sacrificial coatings on steel.

[a] Military Academy, 33 Gen. Pavle Jurisic Sturm St., Belgrade, Serbia
[b] Faculty of Technology and Metallurgy, University of Belgrade, P.O.Box 3503, YU-11120,

## Introduction.

Electrochemical deposition has been well-known method for obtaining metal and alloy coatings, for more than two centuries. Although alternative technologies, like thermal spray coating, vapor deposition, and chemical vapor deposition, have been developed, the electrodeposition is still very popular in an industry, because of many advantages [1]. As an example of the advantage, the chemical composition of binary and ternary electrodeposited alloys can be easily varied by changing the applied electrode potential, electrolyte composition, temperature, etc. [2].

Alloy coatings consisting of two metals, but having different content of each constituent, can extremely differ in surface appearance, morphology, crystallographic structure, and corrosion resistance in aggressive media [3]. The investigations of Zn-Mn alloy deposits, for instance, have shown that the coatings containing 30 - 40 at. % of Mn have significantly higher corrosion resistance as compared to the Zn-Mn alloys with the Mn content of up to 10 at. % [4].

The electrodeposition from the electrolyte consisting of Zn and Mn sulphates, and citrate ligand, enables obtaining Zn-Mn alloy coatings with various Mn contents, namely, in the whole range of 0 – 100 at. %. However, the process has important drawbacks, like poor bath stability and low current efficiency [5]. Contrary, the chloride electrolyte, consisting of Zn and Mn chlorides and boric acid, very successfully copes with the mentioned drawbacks, but on the other hand, only the Zn-Mn alloys with up to approximately 20 at. % of Mn have been successfully deposited from this electrolyte until now [6].

D. Sylla et al. developed a chloride solution for the deposition of Zn-Mn alloys a few years ago [6]. The deposited films had a cauliflower morphology and appeared to be compact and homogeneous. Furthermore, the current efficiency for metal deposition from the chloride solution is very high, near 100%, as a result of boric acid addition, which has been reported to inhibit hydrogen formation, by adsorbing on electrode surface and blocking the active centres for proton reduction [7]. However, it was reported by the authors that a maximum manganese content of only 23 at.% could be reached in the Zn-Mn alloys from chloride solution. Higher Mn content has led to columnar and non-adherent deposits [7].

Correspondingly, the goal of the present study was to obtain such electrodeposition conditions in chloride solution, which would lead to the formation of Zn-Mn films possesing high Mn content, and at the same time compact and homogeneous surface morphology. The alternation of two deposition parameters, namely, deposition current density (c.d.) and manganese concentration in the chloride solution, was investigated. The electrochemical reactions of interest were investigated by cyclic voltammetry and chronoamperometry. The Zn-Mn alloys obtained galvanostatically were characterized by analyzing their composition and morphology.

## Experimental section

Voltammetric experiments were carried out at room temperature in a conventional three-electrode cell, using a potentiostat ZRA Reference 600, Gamry Instruments. The working electrode was a glassy carbon electrode, with the surface area of 0.64 $cm^2$. The reference electrode was a saturated calomel electrode (SCE) mounted in a Luggin capillary. All potentials in this work are referred to this electrode. The counter electrode was a Zn plate (high purity zinc). Voltammetric experiments were carried out at 100 - 600 mV $s^{-1}$, between -1700 mV and 0 mV vs SCE, scanning at first to negative potentials; the initial potential was -500 mV. Only one cycle was run in each voltammetric experiment.

Galvanostatic electrodeposition of Zn-Mn alloys was performed on a steel plates with an active surface area of 3.68 $cm^2$, from chloride solutions which contained 1.8 mol $dm^{-3}$ KCl,

0.4 mol $dm^{-3}$ $H_3BO_3$, 0.4 mol $dm^{-3}$ $ZnCl_2$ and 0.9, 1.8 or 2.4 mol $dm^{-3}$ $MnCl_2 \cdot 4H_2O$. The solution pH was between 4.50 and 5.00. Prior to each experiment, the steel surfaces were abraded successively with emery papers of the following grades: 600, 1000, 1200 and then degreased in a saturated solution of NaOH in ethanol, pickled with a 2 mol $dm^{-3}$ HCl solution for 30 s and finally rinsed with distilled water. The counter and reference electrode were the same as in the voltammetric investigations. The current efficiency was calculated from the weight gain of the samples, so deposition times could be managed to obtain layers with 10 µm thickness.
Surface morphology of the coatings was examined by Scanning electron microscopy (SEM), using a Philips XL30 instrument. Chemical analysis of the deposits was performed by an attached Energy Dispersive X-ray Spectrometer (EDX).

## Results and discussion

### Cyclic voltammetry studies

To determine the effect of manganese salt concentration on the kinetic process of Zn-Mn alloy deposition, voltammetric studies were carried out in solutions containing 1.8 mol $dm^{-3}$ KCl + 0.4 mol $dm^{-3}$ $H_3BO_3$ (blank electrolyte) with 0.9 (solution $S_1$), 1.8 (solution $S_2$), or 2.4 (solution $S_3$) mol $dm^{-3}$ $MnCl_2 \cdot 4H_2O$. Low concentration of $ZnCl_2$ (0.005 mol $dm^{-3}$) was added to all solutions in order to investigate manganese deposition in the presence of zinc. Higher concentration of Zn(II) ions would mask manganese reduction voltammetric peak, because Zn is thermodinamically nobler than Mn [8].
As it was shown by earlier authors [7], a steel electrode is not appropriate for voltammetric study of Mn deposition, because on this substrate, hydrogen evolution occurrs approximately in the same range of potentials as Mn deposition, so it masks the $Mn^{2+}$ reduction contribution. For this reason, cyclic voltammetry studies were performed using a glassy carbon electrode.

### Determination of appropriate potential scan rate

A cyclic voltammograms of glassy carbon electrode, recorded in $S_2$ solution at different potential scan rates, are shown in Fig. 1a. All voltammograms show the same features. When the potential is scanned in the negative direction, the cathodic current begins to increase below -1190 mV and shows a broad peak $C_1$ around -1250 mV, which can be associated to a mass-transport controlled reduction of $Zn^{2+}$. The corresponding anodic stripping peak is the peak $A_1$ at -1035 mV, attributed to the oxidation of metallic zinc into $Zn^{2+}$. [9]. On scanning in the more negative direction, a strong increase in the cathodic current at −1510 mV, with the sharp cathodic peak $C_2$ due to manganese deposition, is observed. Corresponding anodic current peak $A_2$ appears at −1285 mV, attributed to the dissolution of manganese [10]. A further increase in the cathodic current at the forward scan beyond the peak $C_2$, is associated with the beginning of hydrogen evolution on the zinc-manganese deposit. Voltammogram recorded in the blank electrolyte, represented also in the Fig. 1a, clearly shows that hydrogen evolution reaction does not take place on the glassy carbon electrode, in the potential region where metal deposition occurs. However, it should be taken in mind that when Zn and Mn particles are deposited on the glassy carbon electrode, these particles become instantly a substrate where hydrogen evolution reaction can occur more easily at the same potential.
Concerning the influence of the potential scan rate on the Mn deposition, the data in Fig. 1a reveal that an increase in sweep rate shifts the $C_2$ peak potentials to more negative values and increases the $C_2$ peak current. The current of corresponding anodic peak $A_2$ also increases. However, the most important feature of Fig. 1a is that the increase in the current of the $A_2$ peak and the total electric charge below this peak with the increase in the sweep rate, is much sharper than the increase in current and charge related to the peak $C_2$. The current efficiency

of manganese reduction for different sweep rates has been estimated by rationing the electric charge under the cathodic $C_2$ and anodic $A_2$ peak, assuming that the anodic peak corresponds to the amount of the deposited manganese and the cathodic current to both manganese and hydrogen evolution, and the result is presented in Fig. 1b. The appropriate explanation for such an increase in current efficiency with the sweep rate could be the fact that Mn is the most electronegative metal that can be electrodeposited from aqueous solutions, so it is unstable and tends to dissolve easily in acidic media, during the inverse scan [11]. This is non-faradaic dissolution (mass loss without charge transfer associated) so it does not have an associated oxidation current in the voltammogram [12]. The higher sweep rate reduces the time available for Mn self-dissolution and consequently increases the amount of Mn which contributes to the $A_2$ peak current, i.e. the current obtained from faradaic dissolution of manganese. According to these results, the sweep rate value as high as 400 mV $s^{-1}$ was chosen for further experiments, because it enabled us to easily distinguish Mn dissolution peak from the baseline.

The influence of the Mn salt concentration on the Mn deposition

Series of experimentation were carried out to highlight the contribution of Mn salt concentration in the kinetic process of Mn deposition. Fig. 2a shows cyclic voltammograms measured between -1700 mV and 0 mV on glassy carbon electrode, in the solutions $S_1$, $S_2$ and $S_3$ with the sweep rate of 400 mV $s^{-1}$. Starting from the potential of -500 mV in the negative direction scan, all the voltammograms exhibit a slight current onset at -1200 mV, with the diffusional peak at -1250 mV, which was attributed to the Zn deposition in the previous analysis (Fig. 1).

As can be seen in Fig. 2b, in the potential range where Mn reduction starts, the voltammograms exhibit the typical features of a nucleation process of manganese on glassy carbon electrode, which are an increase in current after an induction time and a current loop between the forward and the reverse direction [13]. During the inverse of the potential scan, it is possible to note two crossovers, $E_f$ and $E_c$. The crossover $E_f$ is typical of the formation of a new phase involving a nucleation process. The second crossover potential $E_c$ may be related to the conditional equilibrium potential of couple $Mn^{2+}/Mn^0$ [9]. The $E_c$ crossover potential values for different Mn salt concentrations are presented in Table 1. The standard electrode potential of the couple $Mn^{2+}/Mn^0$ in acidic medium is -1422 mV vs SCE [6], so it is clear from the Table 1 that $Mn^{2+}/Mn^0$ equilibrium potentials in the solutions $S_1$, $S_2$ and $S_3$ are more positive than the standard potential, which is due to high concentrations of Mn(II) species. It is also shown that the increase in Mn salt concentration, shifts the $Mn^{2+}/Mn^0$ equilibrium potential to the more positive values, but the change is very small and it does not obey Nernst equation for the simple reaction

$$Mn^{2+} + 2e = Mn \qquad (1)$$

This is understandable when it is known that in the presence of $Cl^-$ species, several manganese complexes such as $MnCl^+$, $MnCl_2^0$ and $MnCl_3^-$ are susceptible to be formed, and they are characterized by their formation cumulative constants $\beta_1 = 3.85$, $\beta_2 = 1.80$ and $\beta_3 = 0.44$ respectively [10]. According to the formation constants, the free $Mn^{2+}$ species practically do not exist in the solutions $S_1$, $S_2$ and $S_3$, so the manganese reduction mainly occurs through the reduction of Mn-complexes:

$$MnCl_n^{(2-n)} + 2e = Mn + nCl^- \qquad n = 1, 2, 3 \qquad (2)$$

Consequently, $Mn^{2+}/Mn^0$ equilibrium potential values strongly depend on the activity of each complex species as well as free $Cl^-$ species. As a conclusion, cyclic voltammogram results have shown that the solution composition has very low impact on the beginning of the Mn

reduction process, since the difference between the equilibrium $Mn^{2+}/Mn^0$ potentials among all three solutions investigated is only up to 15 mV.

When the electrode reaction is controlled by diffusion processes, there is linear relationship between the peak current intensity ($j_p$) and squared root of the scan rate ($v^{½}$) , and between $j_p$ and the bulk concentration of reducible ions ($c^*$) [14]. Concerning the influence of the potential scan rate (Fig. 1a) and the concentration of Mn(II) ions (Fig. 2a) on the current of the $C_2$ peak associated with the Mn(II) ions reduction, Fig. 3 shows that the $j_p$ - $v^{½}$ relationship is almost ideally linear, but there is no linearity in the $j_p - c^*$ relationship. It suggests that besides the diffusion process, some other process has also strong influence on the Mn reduction. Such process could be the weak complexation of $Mn^{2+}$ ions with the $Cl^-$ species. Furthermore, one should bear in mind that besides the Mn reduction, a large fraction of the $C_2$ peak current comes from the hydrogen evolution reaction on the Zn-Mn deposit.

The current efficiency for Mn reduction from the solutions with different Mn salt concentrations, calculated by rationing the electric charge under the cathodic $C_2$ and anodic $A_2$ peak, is presented in the Table 1. The slight increase in the current efficiency with the Mn salt concentration increase is probably related to the fact that the competitive adsorption between the Mn(II) complexes and $H^+$ ions occurs to occupy active sites for the reduction, so the increase in the Mn(II) ions concentration leads to their preferential adsorption [15].

Cyclic voltammetry studies of manganese electrodeposition on glassy carbon electrode, have shown that the reduction of Mn(II) ions is a partially diffusion - controlled process. Depending on the Mn(II) ion concentration and potential sweep rate applied, limiting diffusion current density (peak $C_2$) is placed in the potential range between -1560 and -1640 mV. It can be suggested that in this potential range, the electrodeposition of Zn-Mn alloys should occur with the highest current efficiency for Mn reduction. Consequently, the chronoamperometric $j - t$ curves for the electrodeposition of Zn-Mn alloys on glassy carbon electrode, were recorded in the mentioned potential range, in the solutions $S_1$‘, $S_2$‘ and $S_3$‘ which were made in the manner that 0.4 mol $dm^{-3}$ $ZnCl_2$ was added to the solutions $S_1$, $S_2$ and $S_3$ respectively. The solutions with the same compositions were used later for the electrodeposition of Zn-Mn alloys on steel substrate. The resulting $j - t$ curves are presented in the Fig. 4. It is seen that shifting the electrodeposition potential from -1550 to -1650 mV enhanced the cathodic reactions in all three solutions. Concerning the influence of the Mn concentration on the deposition current density, it is clearly seen that for the same deposition potential, the absolute value of deposition current density decreases as Mn concentration in the solution increases. For example, at $E$ = -1650 mV, the recorded current density in the solution containing 0.9 mol $dm^{-3}$ $MnCl_2 \cdot 4H_2O$ (solution $S_1$‘) is -290 mA $cm^{-2}$ and in the solution with 2.4 mol $dm^{-3}$ $MnCl_2 \cdot 4H_2O$ (solution $S_3$‘) it is only -160 mA $cm^{-2}$. Such a tendency can be explained again by using the adsorption theory. Since the concentrations of Zn(II) and hydrogen ions near the electrode surface are constant in all three solutions, the increase in concentration of Mn(II) ions enables Mn species to occupy more active sites at the cathode surface, blocking the reduction of hydrogen and Zn ions [15]. The Mn reduction is the slowest process as compared to the hydrogen and Zn ion reduction, so increasing the surface area where the slowest process takes place, decreases the overall measured current density, as Fig. 4 depicts.

Chronoamperometric experiments reveal that the current density for deposition of Zn-Mn alloys corresponding to the potential value where diffusion peak for reduction of Mn(II) species appears, is 290 mA $cm^{-2}$ in the solution $S_1$‘. In solutions with higher Mn ions concentration, the corresponding current densities are even lower. So, it can be concluded that for the purpose of obtaining the Zn-Mn alloys with high Mn content, the reasonable upper limit for the deposition current densities should not be higher than 300 mA $cm^{-2}$.

## Galvanostatic electrodeposition and characterization of the coatings

### Chemical composition of Zn – Mn alloys

The influence of the deposition current density on the Mn content in the alloy is illustrated in Fig. 5 for alloys deposited from solutions with different $Mn^{2+}$ concentrations. The alloy composition was determined by EDX method. Firstly, it can be seen that a sharp increase in Mn content occurs with the increase in deposition c.d. Secondly, it is shown that solutions richer in Mn(II) ions, enable the deposition of coatings with higher Mn content. Both observations are in accordance with the conclusions from cyclic voltammetry. For Zn – Mn alloy electrodeposited from the solution with the lowest content of Mn salt, Mn percentage in the alloy did not reach more than 15 at. %, and it is not presented in Fig. 5. Contrary, when solutions $S_2$' and $S_3$' were investigated, as Fig. 5 depicts, Mn-rich deposits were obtained in the c.d.s range of 200-300 mA $cm^{-2}$. As it was emphasized in the introduction, coatings possessing 30 – 40 at.% of Mn should have the lowest corrosion [4]. Exactly such a chemical composition could be produced under the deposition parameters used in this article.

### SEM characterization

According to the electrochemical study of Zn–Mn electrodeposition, different samples are elaborated on steel electrode, at current densities in the range of 30 – 300 mA $cm^{-2}$, from the solutions containing various Mn(II) concentrations. Several selected samples of Zn-Mn coatings were studied by SEM, and their surface morphologies are shown in Fig. 6. A white bar on micrographs indicates the length of 5, 10, 20 or 50 μm, as it is denoted by the number above the bar.

Examination of the Zn-Mn deposits indicated that the surface morphology of the coatings is affected by the deposition c.d. and Mn content in the solution. Regardless of which solution was employed, the Zn-Mn coatings obtained at *c.d.s* of up to 80 mA $cm^{-2}$ were comprised of the groups of platelets which were found to grow in multilayers (Fig. 6a), typical of pure Zn coatings [16]. At higher deposition *c.d.s,* when Mn content in the alloy is higher, the significant differences are observed for the morphologies obtained from different solutions. Fig. 6b presents the microphotograph of the electrodeposit obtained from the solution containing 0.9 mol $dm^{-3}$ $MnCl_2 \cdot 4H_2O$ (solution $S_1$‘), at 200 mA $cm^{-2}$. A small nodular grains that form some aggregates with fissures between them are observed. Very similar type of morphology was found for the Zn-Mn coatings with 5 – 19 at. % Mn, deposited from the solution which contained Zn(II) and Mn(II) sulphates with some complexing agents [5]. However, in our case, the appearance of this sample is dark, non-adherent and powdery. The morphology of the samples from the $S_1$‘ solution is even worse when higher c.d.s. are applied.

Deposits obtained from the solution which contained 1.8 mol $dm^{-3}$ $MnCl_2 \cdot 4H_2O$ (solution $S_2$‘) at c.d. range of 100 – 200 mA $cm^{-2}$, as well as samples from the solution with 2.4 mol $dm^{-3}$ $MnCl_2 \cdot 4H_2O$ (solution $S_3$‘) deposited at 100 mA $cm^{-2}$, have very different morphology but generally they exhibit a similar appearance: spongy, porous and dark, which is not appropriate for protection coatings. Fig. 6c, for the coating deposited at 200 mA $cm^{-2}$ from the solution $S_2$‘, shows a tree-like dendrites with trunk and branches, which grow with perpendicular orientation to the substrate surface. A dendritic shape is typical for Zn coatings obtained at very negative deposition potentials when the growth process is under mixed diffusion and activation control [17]. A dendritic morphology is observed also at the microphotograph of the sample obtained at 100 mA $cm^{-2}$ from the $S_3$‘ solution (Fig. 6e). In this case, dendrites are made of small hexagonal agglomerations.

However, further increase in deposition c.d. makes remarkable change in the morphology of the Zn-Mn coatings made from the solutions with high Mn content (1.8 and 2.4 mol $dm^{-3}$ $MnCl_2 \cdot 4H_2O$). Coatings become compact, smooth, semi-bright, and with very good adhesion. Microphotographs of these samples (Fig. 6 d, f, g) are similar in shape, with cauliflower-like grains, uniformly and homogeneously distributed. Deposits obtained at 300 mA $cm^{-2}$ from both solutions (Fig. 6 d, g) posses pores with diameter of 1 - 2 μm, probably due to hydrogen evolution during alloy deposition. However, iron, the substrate material, is not detected by EDS analysis on any sample, which proves that the pores are present only on the coating surface, and do not extend into the coating depth [12].
A tin-manganese electrodeposition study by other authors has shown that the increase in deposition c.d. from 100 to 400 mA $cm^{-2}$ induced surface morphology to change from spongy, porous and dark, to bright, glossy and compact [18]. Another investigation of copper-manganese electrodeposits by the same authors show similar improvement in surface morphology as deposition c.d. increases [19]. In both cases, the transition from dendritic to homogeneous and bright appearance is correlated with high Mn percentage present in the alloys. It can be concluded from Figs. 6 a-g that the increase of Mn salt content in the chloride solution used for deposition, lowers the critical deposition c.d. which leads from dendritic to homogeneous and smooth surface morphology. For instance, the transition is not observed at all in the solution with 0.9 mol $dm^{-3}$ of Mn chloride, it is present at 300 mA $cm^{-2}$ when the solution containing 1.8 mol $dm^{-3}$ of Mn chloride is employed, and in the solution with the highest Mn salt content, it is observed already at 200 mA $cm^{-2}$. So, according to the literature and our SEM observations, it is possible that some minimal content of Mn must be present in the Zn-Mn alloy, to obtain good surface appearance, which is the same behaviour as with Sn-Mn and Cu-Mn coatings.

## Conclusion

On the basis of the results presented it could be concluded that a ratio of manganese to zinc ions in the plating solution and deposition current density, have significant influence on the chemical composition and the morphology of Zn–Mn electrodeposited alloys. High deposition current densities applied in the solutions with high $Mn^{2+}$ concentration, enable producing high-Mn Zn-Mn deposits. These coatings have shown to have smooth, adherent, bright and homogeneous morphology, and could be used as sacrificial films on steel.

## References

[1] C.T.J. Low, R.G.A. Wills, F.C. Walsh, Electrodeposition of composite coatings containing nanoparticles in a metal deposit, Surf. Coat. Technol. 201 (2006) 371-383.

[2] V.D. Jović, B.M. Jović, M.G. Pavlović, Electrodeposition of Ni, Co and Ni–Co alloy powders, Electrochim. Acta 51 (2006) 5468–5477.

[3] J.B. Bajat, S. Stanković, B.M. Jokić, S.I. Stevanović, Corrosion stability of Zn–Co alloys deposited from baths with high and low Co content - The influence of deposition current density, Surf. Coat. Technol. 204 (2010) 2745–2753.

[4] B. Bozzini, E. Griskonis, A. Fanigliulo, A. Sulcius, Electrodeposition of Zn–Mn alloys in the presence of thiocarbamide, Surf. Coat. Technol. 154 (2002) 294-303.

[5] C. Muller, M. Sarret, T. Andreu, Electrodeposition of Zn-Mn Alloys at low current densities, J. Electrochem. Soc. 149 (2002) C600-C606.

[6] D. Sylla, J. Creus, C. Savall, O. Roggy, M. Gadouleau, Ph. Refait, Electrodeposition of Zn–Mn alloys on steel from acidic Zn–Mn chloride solutions, Thin Solid Films 424 (2003) 171-178.

[7] C. Savall , C. Rebere, D. Sylla, M. Gadouleau, Ph. Refait, J. Creus, Morphological and structural characterisation of electrodeposited Zn–Mn alloys from acidic chloride bath, Mat. Sci. Eng. A 430 (2006) 165–171.

[8] P. Díaz-Arista, Z.I. Ortiz, H. Ruiz, R. Ortega, Y. Meas, G. Trejo, Electrodeposition and characterization of Zn–Mn alloy coatings obtained from a chloride-based acidic bath containing ammonium thiocyanate as an additive, Surf. Coat. Technol. 203 (2009) 1167–1175.

[9] A. Gomes, M.I. da Silva Pereira, Zn electrodeposition in the presence of surfactants: Part I. Voltammetric and structural studies, Electrochim. Acta 52 (2006) 863–871.

[10] B. Benfedda, N. Benbrahim, A. Kadri, E. Chainet, F. Charlot, S. Coindeau, Electrodeposition and characterization of manganese–bismuth system from chloride based acidic bath, Electrochim. Acta 56 (2011) 1275–1282.

[11] J. Gong, G. Zangari, Electrodeposition and Characterization of Manganese Coatings , J. Electrochem. Soc. 149 (2002) C209.

[12] P. Diaz-Arista, R. Antano Lopez, Y. Meas, R. Ortega, E. Chainet, P. Ozil, G. Trejo, EQCM study of the electrodeposition of manganese in the presence of ammonium thiocyanate in chloride-based acidic solutions, Electrochim. Acta 51 (2006) 4393–4404.

[13] E. Gomez, E. Pelaez, E. Valles, Electrodeposition of zinc+iron alloys: I. Analysis of the initial stages of the anomalous codeposition, J. Electroanal. Chem. 469 (1999) 139–149.

[14] J. Zhang, M. An, L. Chang, Study of the electrochemical deposition of Sn–Ag–Cu alloy by cyclic voltammetry and chronoamperometry, Electrochim. Acta 54 (2009) 2883–2889.

[15] M.M. Abou Krisha, F.H. Assaf, A.A. Toghan, Electrodeposition of Zn–Ni alloys from sulfate bath, J. Solid State Electrochem. 11 (2007) 244-252.

[16] L.E. Moron, A. Mendez, F. Castaneda, J.G. Flores, L. Ortiz-Frade, Y. Meas, G. Trejo, Electrodeposition and characterization of Zn–Mn alloy coatings obtained from a chloride-based acidic bath containing ammonium thiocyanate as an additive, Surf. Coat. Technol. 205 (2011) 4985–4992.

[17] Y.F. Lin, I.W. Sun, Electrodeposition of zinc from a Lewis acidic zinc chloride-1-ethyl-3-methylimidazolium chloride molten salt, Electrochim. Acta 44 (1999) 2771-2777.

[18] J. Gong, G. Zangari, Electrodeposition of sacrificial tin–manganese alloy coatings, Mat. Sci. Eng. A 344 (2003) 268-278.

[19] J. Gong, G. Wei, J.A. Barnard, G. Zangari, Electrodeposition and characterization of sacrificial copper-manganese alloy coatings: Part II. Structural, mechanical, and corrosion-resistance properties, Metallurgical and Materials Transactions A 36 (2005) 2705-2715.

Table 1. The potential crossover ($E_c$), current density for peak $C_2$ ($j_p$), cathodic charge under the peak $C_2$ ($Q_c$) and anodic charge under the peak $A_2$ ($Q_a$), obtained from the voltammograms in the Fig. 2a.

| $c$ ($MnCl_2 \cdot 4H_2O$) | $E_c$, mV | $j_p$, mA cm$^{-2}$ | $Q_c$, mC cm$^{-2}$ | $Q_a$, mC cm$^{-2}$ | *current efficiency*, % |
|---|---|---|---|---|---|
| 0.9 mol dm$^{-3}$ | -1399 | -85.16 | -22.61 | 1.76 | 7.8 |
| 1.8 mol dm$^{-3}$ | -1399 | -151.68 | -34.39 | 7.08 | 20.6 |
| 2.4 mol dm$^{-3}$ | -1384 | -168.44 | -47.50 | 13.14 | 27.7 |

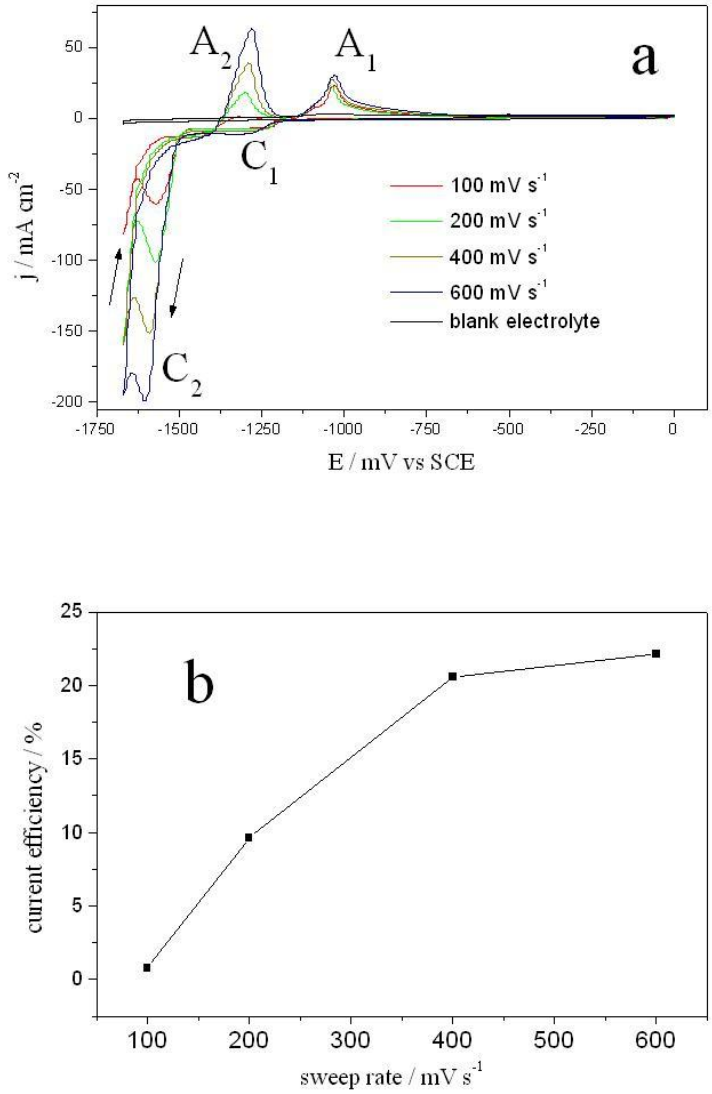


**Fig. 1. a)** Cyclic voltammograms for glassy carbon electrode in 1.8 mol dm$^{-3}$ KCl + 0.4 mol dm$^{-3}$ $H_3BO_3$ (blank electrolyte) + 1.8 mol dm$^{-3}$ $MnCl_2 \cdot 4H_2O$ + 0.005 mol dm$^{-3}$ $ZnCl_2$, at various potential sweep rates; b) variation of current efficiency for Mn deposition with the sweep rate.

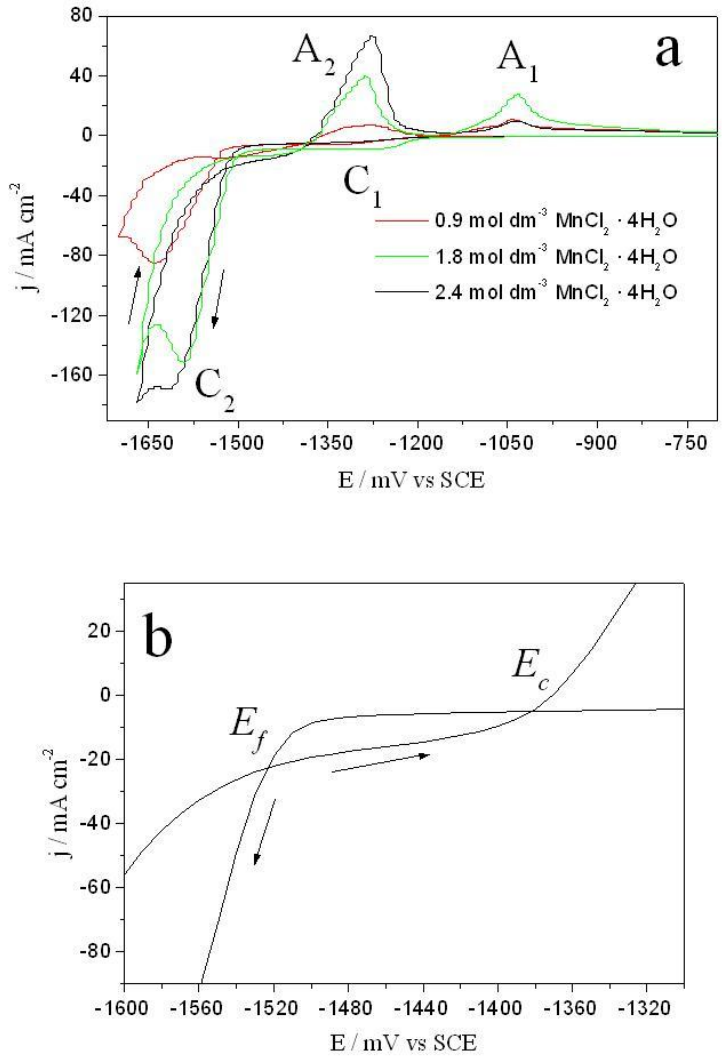


**Fig. 2. a)** Cyclic voltammograms obtained for glassy carbon electrode at scanning rate 400 mV $s^{-1}$ in basic solution + 0.005 mol $dm^{-3}$ $ZnCl_2$ + various concentrations of $MnCl_2 \cdot 4H_2O$; b) magnified part of voltammogram in solution with 2.4 mol $dm^{-3}$ $MnCl_2 \cdot 4H_2O$.

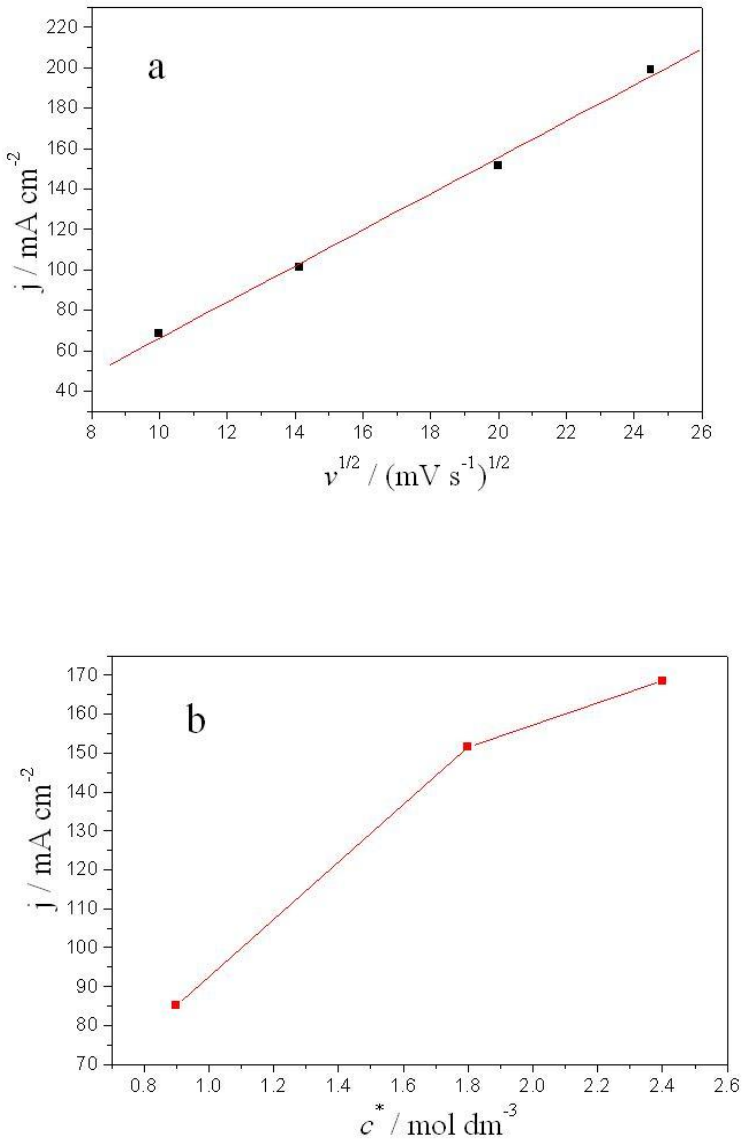


**Fig. 3.** Variation of current density for peak $C_2$ with squared root of the potential scan rate (a) and bulk concentration of Mn(II) species (b).

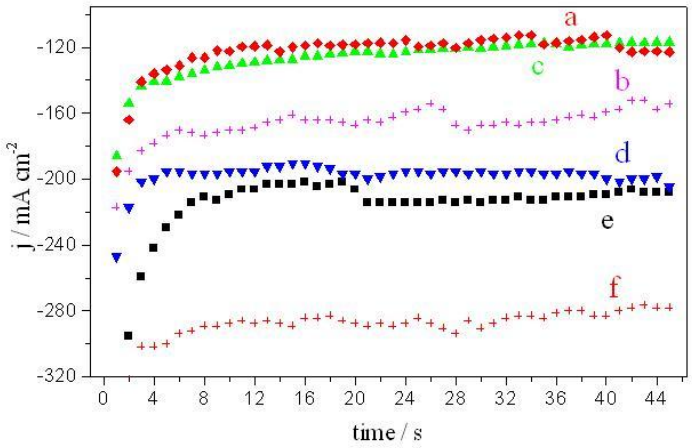


**Fig. 4.** Current density –time transients for Zn-Mn films deposited on glassy carbon substrate in basic solution with 0.4 mol $dm^{-3}$ $ZnCl_2$ and 2.4 mol $dm^{-3}$ $MnCl_2 \cdot 4H_2O$ (a) E = −1550 mV, (b) E = −1650 mV; 1.8 mol $dm^{-3}$ $MnCl_2 \cdot 4H_2O$ (c) E = −1550mV, (d) E = −1650 mV; and 0.9 mol $dm^{-3}$ $MnCl_2 \cdot 4H_2O$ (e) E = −1550 mV, (f) E = −1650 mV.

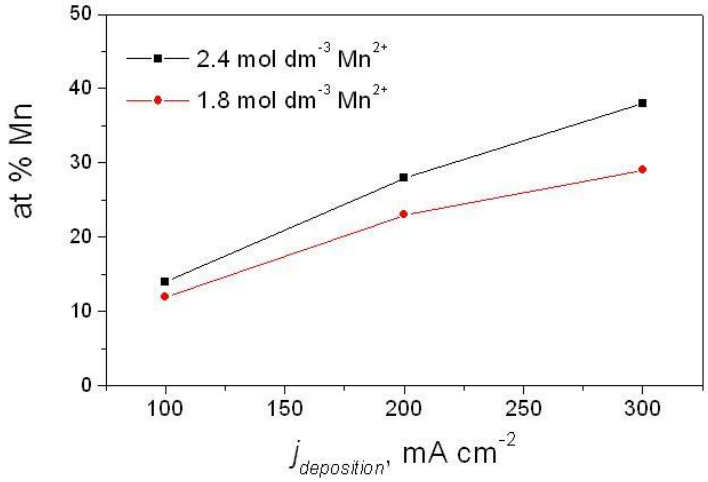


Fig. 5. The influence of deposition current density on chemical composition of Zn-Mn alloys

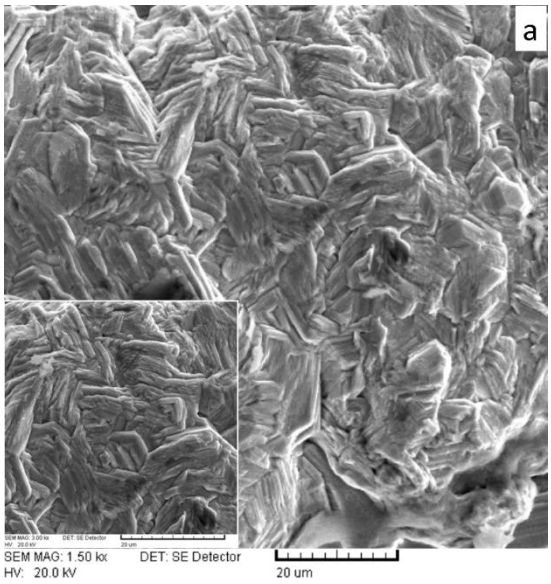
a
SEM MAG: 1.50 kx
HV: 20.0 kV
DET: SE Detector
20 um

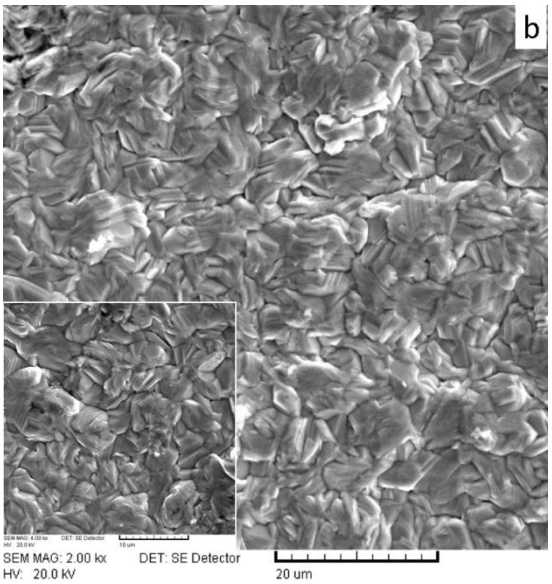
b
SEM MAG: 2.00 kx
HV: 20.0 kV
DET: SE Detector
20 um

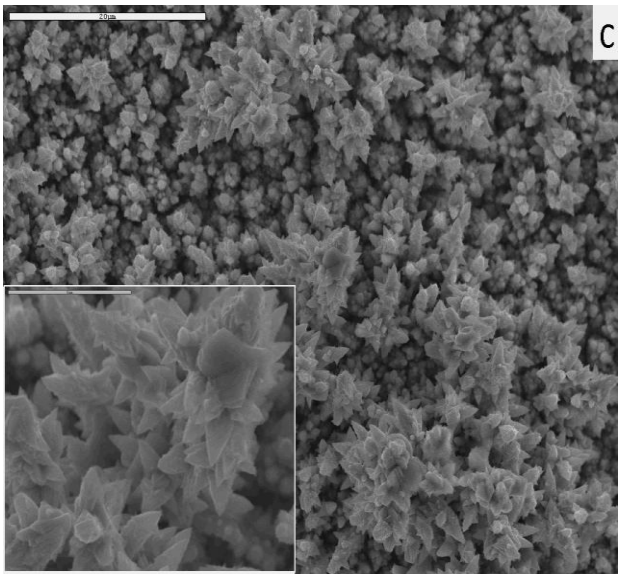
c

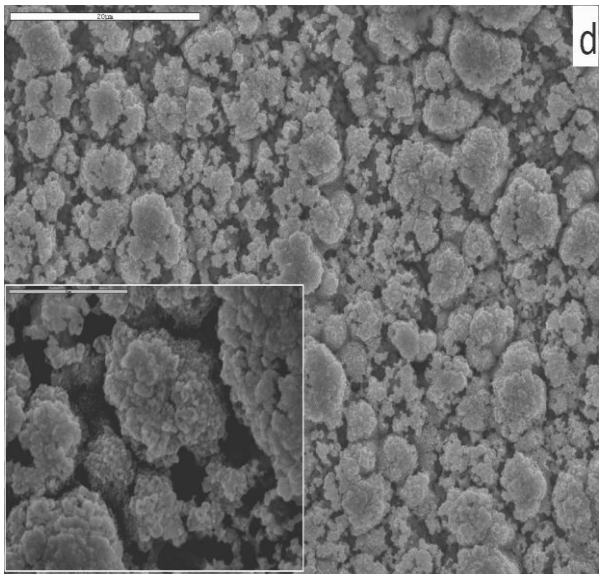
d

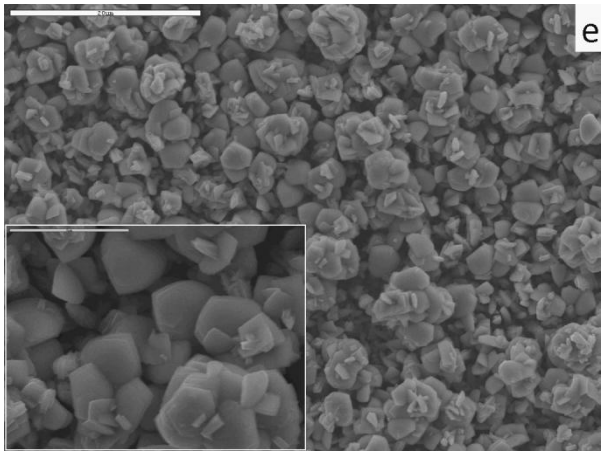
e

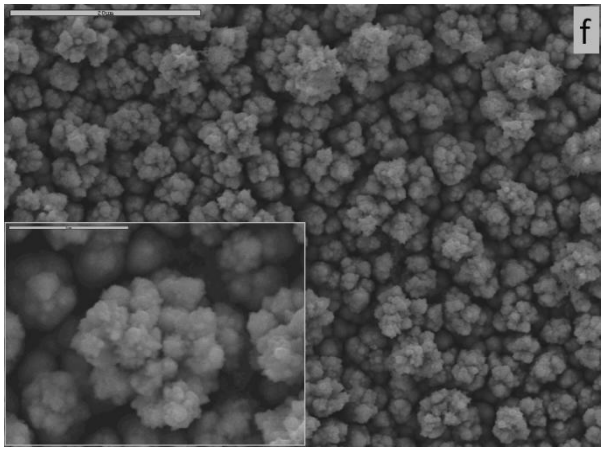
f

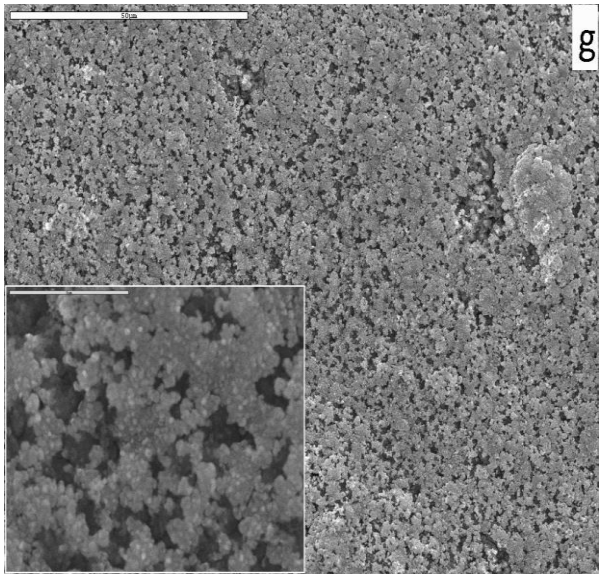


**Fig. 6.** SEM images of Zn-Mn coatings formed from the solution $S_1$' at 30 mA $cm^{-2}$ (a) and 200 mA $cm^{-2}$ (b), solution $S_2$' at 200 mA $cm^{-2}$ (c) and 300 mA $cm^{-2}$ (d), and solution $S_3$' at 100 mA $cm^{-2}$ (e), 200 mA $cm^{-2}$ (f) and 300 mA $cm^{-2}$ (g).